High-Surface-Area Catalyst Design: Synthesis, Characterization, and Reaction Studies of Platinum Nanoparticles in Mesoporous SBA-15 Silica†

R. M. Rioux,‡ H. Song,‡ J. D. Hoefelmeyer, P. Yang,* and G. A. Somorjai*

Department of Chemistry, University of California, Berkeley, and Materials Science Division, Lawrence Berkeley National Laboratory, Berkeley, California 94720

Received: March 14, 2004; In Final Form: June 6, 2004

Platinum nanoparticles in the size range of 1.7−7.1 nm were produced by alcohol reduction methods. A polymer (poly(vinylpyrrolidone), PVP) was used to stabilize the particles by capping them in aqueous solution. The particles were characterized by X-ray diffraction (XRD) and transmission electron microscopy (TEM). TEM investigations demonstrate that the particles have a narrow size distribution. Mesoporous SBA-15 silica with 9-nm pores was synthesized by a hydrothermal process and used as a catalyst support. After incorporation into mesoporous SBA-15 silica using low-power sonication, the catalysts were calcined to remove the stabilizing polymer from the nanoparticle surface and reduced by H_2. Pt particle sizes determined from selective gas adsorption measurements are larger than those determined by bulk techniques such as XRD and TEM. Room-temperature ethylene hydrogenation was chosen as a model reaction to probe the activity of the Pt/SBA-15 materials. The reaction was shown to be structure insensitive over a series of Pt/SBA-15 materials with particle sizes between 1.7 and 3.6 nm. The hydrogenolysis of ethane on Pt particles from 1.7 to 7.1 nm was weakly structure sensitive with smaller particles demonstrating higher specific activity. Turnover rates for ethane hydrogenolysis increased monotonically with increasing metal dispersion, suggesting that coordinatively unsaturated metal atoms present in small particles are more active for C_2H_6 hydrogenolysis than the low index planes that dominate in large particles. An explanation for the structure sensitivity is suggested, and the potential applications of these novel supported nanocatalysts for further studies of structure−activity and structure−selectivity relationships are discussed.

1 Introduction

One of the goals of catalysis research is to design and fabricate a catalyst system that produces only one desired product out of many other possible products (100% selectivity) at high turnover rates. Such a "green chemistry" process eliminates the production of undesirable waste. To design a catalyst for the "green chemistry" era, an understanding of the molecular ingredients that influence selectivity must be incorporated into catalyst synthesis. Using model catalysts possessing low surface area (1 cm^2 metal single crystals) and 2-D transition metal/metal oxide array catalysts, many of the molecular features that control activity and selectivity have been uncovered. These include the surface structure,[1] metal particle size,[2] site blocking (i.e., selective poisoning of the catalyst surface),[3] bifunctional catalytic systems,[4] and certain metal−oxide interfaces[5] capable of performing unique chemistry. One of the most mature areas of selectivity control in heterogeneous catalysis is shape-selective zeolite catalysis.[6] Reaction selectivity is imparted by restricting the entry channel to the internal zeolite structure to molecular diameters which are smaller than the diameter of some potential reactants and products, requiring product formation to occur in a shape-selective manner.

We have recently initiated research to design high-surface-area catalysts[7,8] whose properties can be controlled systematically and ultimately allow us to determine the role of various parameters on reaction activity and selectivity. Departing from the traditional catalytic synthetic techniques (i.e., incipient wetness, ion exchange), we have developed a synthetic method which allows precise control of the metal particle size and tuning of the mesoporous SBA-15 silica support pore diameter (Figure 1). Control of the Pt particle size is achieved with solution-based alcohol reduction methods. Platinum nanoparticles in the 1.7−7.1-nm range have been synthesized and incorporated into a mesoporous silicate support using low-power sonication that facilitates Pt particle entry into the SBA-15 channels by capillary inclusion. After synthesis, the catalysts were characterized by both physical and chemical techniques, such as transmission electron microscopy (TEM), X-ray diffraction (XRD), low-angle XRD, physical adsorption, and chemisorption of probe gases to determine metal surface area. Chemisorption of probe gases demonstrated that the stabilizing polymer used during nanoparticle synthesis could be removed after appropriate thermal treatment. These Pt/SBA-15 materials are active for two hydrocarbon test reactions, C_2H_4 hydrogenation and C_2H_6 hydrogenolysis. Reaction kinetics are compared with results obtained using two-dimensional single crystals, nanoparticle arrays deposited on silica, and with classical high-surface-area supported platinum catalysts. This study represents a new

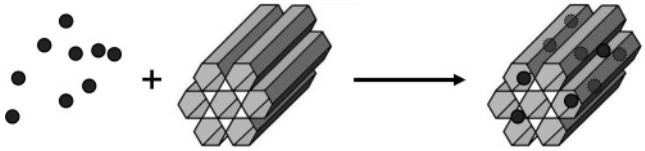

Figure 1. Synthetic scheme for the inclusion method.

† Part of the special issue "Michel Boudart Festschrift".

* Authors to whom correspondence should be addressed. E-mail: somorjai@cchem.berkeley.edu, p_yang@cchem.berkeley.edu.

‡ These authors contributed equally to this work.

10.1021/jp048867x CCC: $30.25
Published on Web 08/12/2004

strategy in catalyst design that utilizes nanoscience to fabricate active catalyst sites, which are deposited on a support to produce a model heterogeneous catalyst. The precise control obtained in these catalytic systems may enable very accurate structure−activity or more importantly structure−selectivity correlations to be established, which will be the direction of future research.

2 Experimental Section

2.1 Pt Nanoparticle Synthesis. Hexachloroplatinic acid, $H_2PtCl_6 \cdot 6H_2O$ (99.9%, metals basis) was purchased from Alfa Aesar. Poly(vinylpyrrolidone) (PVP, $M_w = 29\,000$ and 55 000) was obtained from Aldrich. Methanol, ethanol, and ethylene glycol were used without further purification. Platinum particles from 1.7 to 3.6 nm were synthesized according to literature methods.[9,10] The synthesis of Pt nanoparticles in the size range 1.7−7.1 nm is briefly summarized.

1.7-nm Pt Particles. NaOH (12.5 mL, 0.5 M) in ethylene glycol was added to a solution of $H_2PtCl_6 \cdot 6H_2O$ (0.25 g, 0.48 mmol) in 12.5 mL of ethylene glycol. The mixture was heated at 433 K for 3 h accompanied by N_2 bubbling. A 6-mL aliquot of the resulting solution was transferred to a vial. The particles were precipitated by adding 1 mL of 2 M HCl, and dispersed in ethanol containing 12.2 mg of PVP ($M_w = 29\,000$). The solvent was evaporated and the residue was redispersed in water.

2.6-nm Pt Particles. PVP (133 mg) was dissolved in a mixture of 20 mL of 6.0 mM $H_2PtCl_6 \cdot 6H_2O$ aqueous solution and 180 mL of ethanol. The mixture was refluxed for 3 h. The solvent was evaporated, and the residue was redispersed in water.

2.9-nm Pt Particles. PVP (133 mg) was dissolved in a mixture of 20 mL of 6.0 mM $H_2PtCl_6 \cdot 6H_2O$ aqueous solution and 180 mL of methanol. The reaction condition was the same as that for 2.6-nm particles.

3.6-nm Pt Particles. Freshly prepared 2.9-nm Pt colloidal solution (100 mL) in a water/methanol (1:9) mixture was mixed with 10 mL of 6.0 mM $H_2PtCl_6 \cdot 6H_2O$ solution and 90 mL of methanol. The reaction condition was the same as those for 2.6- and 2.9-nm particles.

7.1-nm Pt Particles. A total 3 mL of 0.375 M PVP ($M_w = 55\,000$) and 1.5 mL of 0.0625 M $H_2PtCl_6 \cdot 6H_2O$ (PVP/Pt salt = 12:1) solutions in ethylene glycol were alternatively added to 2.5 mL of boiling ethylene glycol every 30 s over 16 min. The reaction mixture was refluxed for additional 5 min. The particles were precipitated by adding triple volume of acetone, and redispersed in water. All Pt colloidal solutions were adjusted to 3×10^{-3} M based on the Pt salt concentration by adding appropriate amount of deionized water.

2.2 Synthesis of Mesoporous SBA-15 Silica. Silica SBA-15 was prepared according to the method reported in the literature.[11] Pluronic P123 (BASF, $EO_{20}PO_{70}EO_{20}$, EO = ethylene oxide, PO = propylene oxide) and tetraethoxysilane (TEOS, 99+%, Alfa Aesar) were used as received. Pluronic P123 (6 g) was dissolved in 45 g of water and 180 g of 2 M HCl solution with stirring at 308 K for 30 min. TEOS (12.75 g) was added to the solution with stirring at 308 K for 20 h. The mixture was aged at 373 K for 24 h. The white powder was recovered through filtration, washed with water and ethanol thoroughly, and dried in air. The product was calcined at 823 K for 12 h to produce SBA-15 with a pore diameter of 9 nm. The final calcined material had a surface area of 765 $m^2\ g^{-1}$ and a pore volume of 1.16 $cm^3\ g^{-1}$.

2.3 Preparation of Pt/SBA-15. Pt colloidal aqueous solution (25.6 mL, 3×10^{-3} M) was mixed with 74.4 mL of water and 100 mL of ethanol. The mixture was quickly added to 1.5 g of SBA-15, and the slurry was sonicated for 3 h at room temperature by a commercial ultrasonic cleaner (Branson, 1510R-MT, 70 W, 42 kHz). The brown precipitates were separated by centrifugation, thoroughly washed with water and ethanol, and dried in an oven at 373 K. Pt (1.7 nm)/SBA-15 was calcined at 623 K for 12 h, Pt (7.1 nm)/SBA-15 was calcined at 723 K for 24 h, and all other catalysts were calcined at 723 K for 12 h with O_2 flow.

2.4 Catalyst Characterization. TEM experiments were made on a Topcon EM002B microscope operated at 200 kV at the National Center for Electron Microscopy at Lawrence Berkeley National Laboratory. Aqueous Pt colloidal solutions were dropped and dried on carbon-film-coated copper grids (Ted Pella). Dried SBA-15 and Pt/SBA-15 powders were sonicated in acetone for several seconds, dropped on the TEM grids, and dried in air. A minimum of two hundred particles were counted for determination of a number-average particle size. XRD patterns were measured on a Bruker D8 GADDS diffractometer using Co Kα radiation (1.79 Å). Low-angle XRD patterns were recorded on a Siemens D5000 diffractometer using Cu Kα radiation (1.54 Å). Nitrogen porosimetry data were collected on a Quantachrome Autosorb-1 analyzer at 77 K. Elemental analyses were conducted at Galbraith Laboratories, Inc.

Selective gas adsorption measurements were measured in a volumetric apparatus constructed of Pyrex that obtained a pressure below 5×10^{-6} Torr in the sample cell by use of a liquid nitrogen trapped diffusion pump (Varian M2). The amount of adsorbed gas was monitored using a digital pressure gauge (MKS, model PDR-D). Total and reversible isotherms were measured with an interim 1-h evacuation between isotherms. The amount of adsorbed gas was extrapolated to zero pressure for all adsorbates. Catalysts were reduced at 673 K for 75 min and evacuated at 623 K for 1 h prior to any chemisorption measurement at 295−300 K. H_2 (Matheson, UHP), O_2 (Airgas, UHP), and CO (Matheson, UHP, Al cylinder) were all used without further purification for chemisorption measurements.

2.5 Reaction Studies. The hydrogenation of ethylene was conducted at 273−313 K in a plug flow reactor (PFR) constructed of Pyrex. Gas flow rates were controlled by mass flow controllers (Unit instruments) connected to a central manifold of $^1/_4$-in. stainless steel tubing. Ethylene (Airgas CP grade), H_2 (Matheson, UHP), and He (Matheson, UHP) were used without further purification. Gas-phase concentrations were determined by gas chromatography (HP 5890) using an FID detector and isothermal temperature program with a homemade alumina column (6 ft. × $^1/_8$-in. o.d.). The total conversion of ethylene was <10% for all temperatures studied. Typically, catalysts were diluted with low-surface-area (2.5 $m^2\ g^{-1}$) acid-washed quartz in a 1:3 catalyst-to-quartz ratio. Room-temperature ethylene hydrogenation required 1−3 mg of catalyst. The effect of dilution on catalyst performance was tested[12] and it was verified that dilution ratios less than 10 had no effect on catalyst activity. Lack of heat and mass transfer limitations were confirmed by use of the Madon−Boudart test[13] at 273 and 298 K for Pt (3.6 nm)/SBA-15 with three different Pt loadings. Kinetic parameters on the reduced catalysts were measured as well as reaction orders in ethylene and hydrogen at various temperatures. Turnover rates in this paper are reported at standard conditions of 10 Torr C_2H_4, 100 Torr H_2, and 298 K. During all kinetic measurements, the last point was duplicated to verify that deactivation had not occurred during the course of the experiment.

Hydrogenolysis of ethane (Airgas, UHP) was studied from 613 to 653 K in a differentially operated plug flow reactor (PFR). At standard conditions of 20 Torr C_2H_6 and 200 Torr

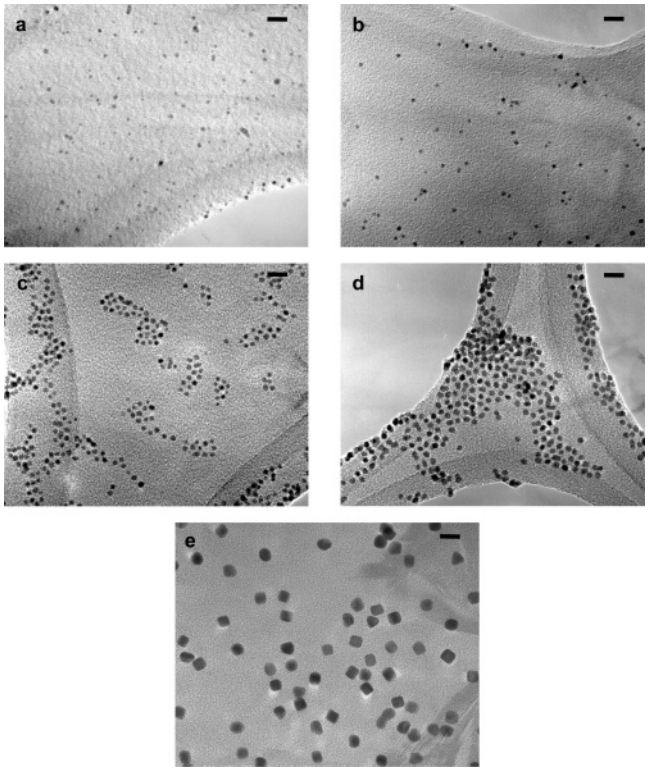

Figure 2. TEM images of the Pt particles of (a) 1.7 nm, (b) 2.6 nm, (c) 2.9 nm, (d) 3.6 nm, and (e) 7.1 nm. The scale bars represent 10 nm.

H_2, all conversions were <5% for the entire temperature range examined. Reaction orders in ethane and hydrogen were collected for Pt (*X*)/SBA-15 catalysts at 643 K with particle sizes (*X*) ranging from 1.7 to 7.1 nm.

3 Results and Discussion

3.1 Synthesis and Characterization of Pt Particles. Monodisperse Pt particles of 1.7−3.6 nm were synthesized by modified alcohol reduction methods according to the literature.[9,10] Methanol, ethanol, and ethylene glycol served as solvents for dissolving Pt salts and PVP, and as a reducing agent of Pt according to the following reaction:

$$H_2PtCl_6 + 2\,RCH_2OH \rightarrow Pt^0 + 2RCHO + 6HCl$$

Pt particle size increases from 1.7 to 2.9 nm as the reaction temperature decreases from 433 K in ethylene glycol to 338 K in boiling methanol. This indicates that reduction of the Pt salts at high temperature produces more Pt nuclei in a short period and eventually affords smaller Pt particles. The 3.6-nm Pt particles were successfully obtained by addition of 2.9-nm particles as a seed for stepwise growth. The 7.1-nm Pt particles were generated by slow and continuous addition of the Pt salt and PVP to boiling ethylene glycol, described elsewhere in detail.[14] All aqueous Pt colloidal solutions with PVP are stable for more than two weeks.

Pt particle sizes were measured by XRD and TEM. Figure 2 shows that the particles are uniform and have a narrow size distribution. An example of the particle size distribution for free-standing 2.9-nm particles is shown in Figure 3. Average Pt particle sizes estimated by XRD (Figure 4) are 1.7, 2.6, 2.9, 3.6, and 7.1 nm, and match very well with TEM results (1.73±0.26, 2.48±0.22, 2.80±0.21, 3.39±0.26, and 7.16±0.37 nm).

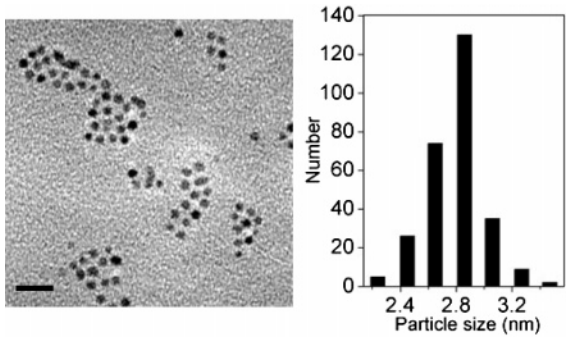

Figure 3. TEM image and particle size histogram for free-standing 2.9 nm Pt particles. The number-average Pt particle size was obtained by counting 281 particles.

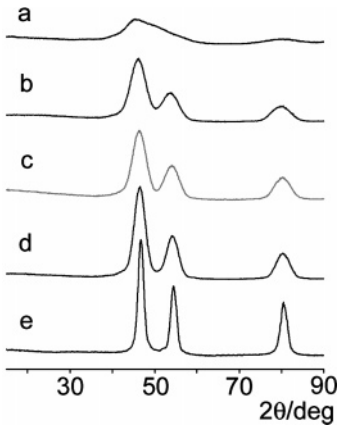

Figure 4. XRD data for free-standing Pt particles of (a) 1.7 nm, (b) 2.6 nm, (c) 2.9 nm, (d) 3.6 nm, and (e) 7.1 nm.

3.2 Synthesis and Characterization of Pt/SBA-15 Catalysts. *3.2.1 Incorporation of the Pt Particles in SBA-15 Structure.* SBA-15 with a pore diameter of 9.0 nm was used as a catalyst support due to its high surface area (700−800 $m^2\ g^{-1}$) and ordered mesoporous structure.[11] Platinum particles of different sizes were dispersed in a 1:1 mixture of water and ethanol, and mixed with SBA-15 under sonication for 3 h at room temperature. After calcination at 723 K with O_2 flow, ca. 1 wt. % Pt(*X*)/SBA-15 catalysts ($X = 1.7$, 2.6, 2.9, 3.6, and 7.1 nm) were obtained as pale brown powders. These materials were characterized by XRD, TEM, and physisorption measurements. TEM images of Pt/SBA-15 samples (Figure 5) show that the particles are well-dispersed in the entire channel structures even for the largest Pt particles (7.1 nm). Three Pt reflections are seen in the XRD patterns of SBA-15 catalysts (Figure 6). These peaks are observed at $2\theta = 45.9°$, 54.0°, and 80.1° assignable to (111), (200), and (220) reflections of the fcc Pt lattice, respectively, as well as a very broad signal at $2\theta = 27.4°$ for amorphous SiO_2. As the particle size increases, characteristic reflections of the Pt lattice become sharper as expected. The particle sizes for Pt incorporated into the support were calculated from the full width at half-maximum (fwhm) of the Pt(111) peak after baseline subtraction of pristine SBA-15. Particle sizes are almost identical to those of the free-standing Pt particles in solution. Low-angle XRD patterns (Figure 7) for all Pt/SBA-15 catalysts exhibit three characteristic peaks indexed as (100), (110), and (200) of the two-dimensional *p*6*mm* hexagonal mesostructure with d_{100} spacing of 10.1 nm, similar to pristine SBA-15.[11] Measured BET surface areas of the catalysts are 690−830 $m^2\ g^{-1}$, while pore volumes are 1.08−1.31 $cm^3\ g^{-1}$. BET isotherms of the samples before and after inclusion of 2.9-nm Pt particles on SBA-15 are shown in Figure 8, and

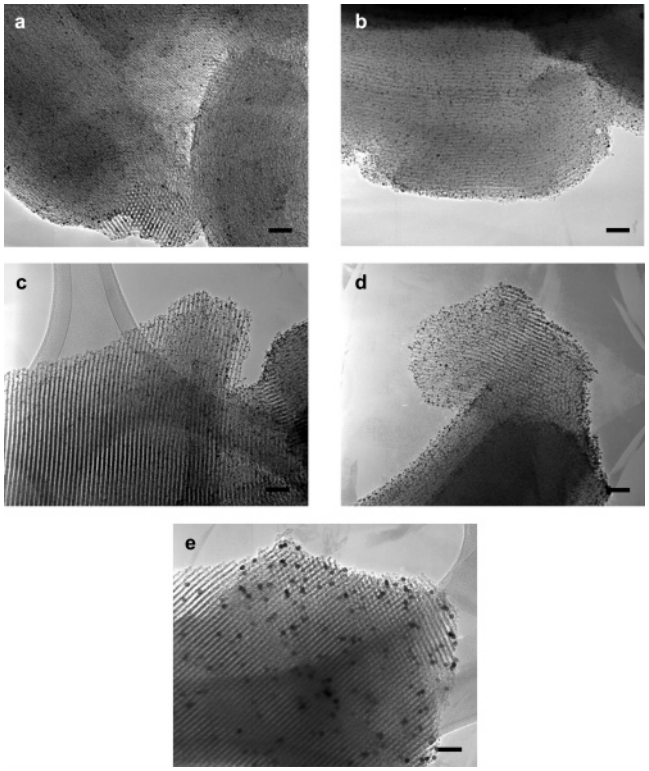

Figure 5. TEM images of the Pt(*X*)/SBA-15 catalysts: X = (a) 1.7 nm, (b) 2.6 nm, (c) 2.9 nm, (d) 3.6 nm, and (e) 7.1 nm. The scale bars represent 20 nm.

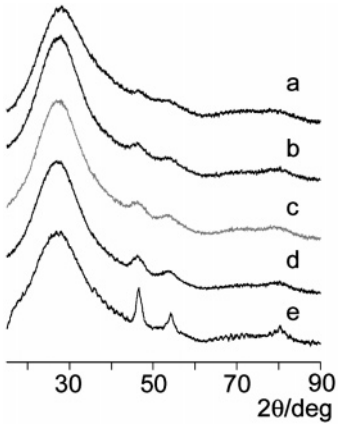

Figure 6. XRD data of the Pt(*X*)/SBA-15 catalysts: X = (a) 1.7 nm, (b) 2.6 nm, (c) 2.9 nm, (d) 3.6 nm, and (e) 7.1 nm.

demonstrate that the inclusion process does not disrupt the SBA-15 mesostructure. Low-angle XRD data and TEM images indicate that the hexagonal wall structure of SBA-15 is robust under the conditions of catalyst synthesis. The minimal change in SBA-15 physical parameters after incorporation of Pt into the silica reveals that there is no significant blocking of the SBA-15 channel by Pt particles.

3.2.2 Efficient Incorporation of Pt Nanoparticles in SBA-15. For homogeneous dispersion of the Pt particles within the silica channels, sonication of the reaction mixture is required. Without sonication, particles are primarily attached on the external surface of SBA-15 and become large aggregates after high-temperature treatment. The extent of Pt dispersion with the SBA-15 framework was followed with time by TEM (Figure 9). Pt particles were rapidly adsorbed on the external surface of SBA-15 within 3 min, followed by diffusion of the Pt particles into the channels over 1.5 h, and finally dispersed throughout the

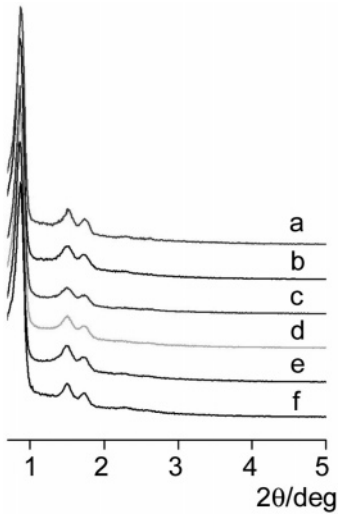

Figure 7. Low-angle XRD patterns of (a) pristine SBA-15, and ~1% Pt(*X*)/SBA-15: X = (b) 1.7 nm, (c) 2.6 nm, (d) 2.9 nm, (e) 3.6 nm, and (f) 7.1 nm.

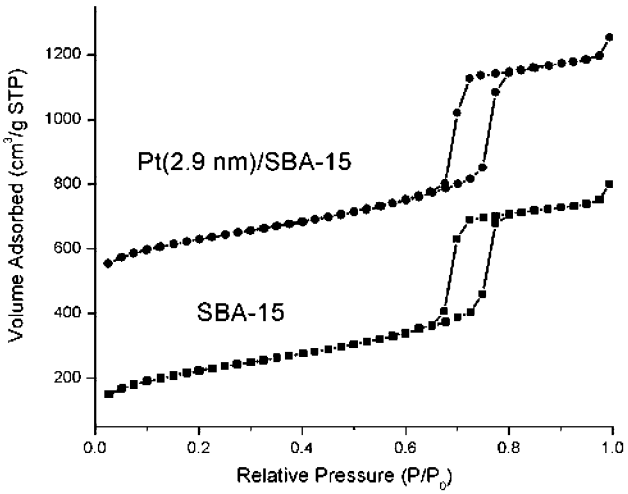

Figure 8. Nitrogen adsorption isotherms of SBA-15 and Pt (2.9 nm)/SBA-15. The isotherm for Pt (2.9 nm)/SBA-15 is shifted by 400 cm^3/g STP.

entire SBA-15 channel. Sonication effectively prevents Pt particles from blocking the pore entrance, promoting homogeneous inclusion. A proper choice of the inclusion solvent should also be considered. In pure water rather than a water/ethanol (1:1) mixture, Pt particles were mainly deposited on the outer surface of SBA-15 after sonication for 3 h, eventually leading to large aggregates after calcination. Huang et al. reported similar phenomenon for Ag nanowire formation within SBA-15 channels,[15] and suggested that it is attributed to the different surface tensions of H_2O (71.99 mN m^{-1}) and ethanol (21.97 mN m^{-1}).

The location of nanoparticles is an important issue in these metal/mesoporous silica catalysts. Janssen et al. imaged three-dimensional structures of metal and metal oxide particles in SBA-15 by bright-field electron tomography, but the results were difficult to interpret due to diffraction contrast.[16] The ordering of Pt nanoparticles within the silica channels was visualized by synthesizing a Pt (2.9 nm)/SBA-15 with a high metal content (14.4 wt %). Figure 10a shows that the silica channels are filled with a significant number of small particles appearing as black stripes. After treatment at 673 K for 75 min with H_2 flow (Figure 10b), nearest neighbor particles aggregated to form nanorods in conformation with the geometry of the SBA-15 channel. This

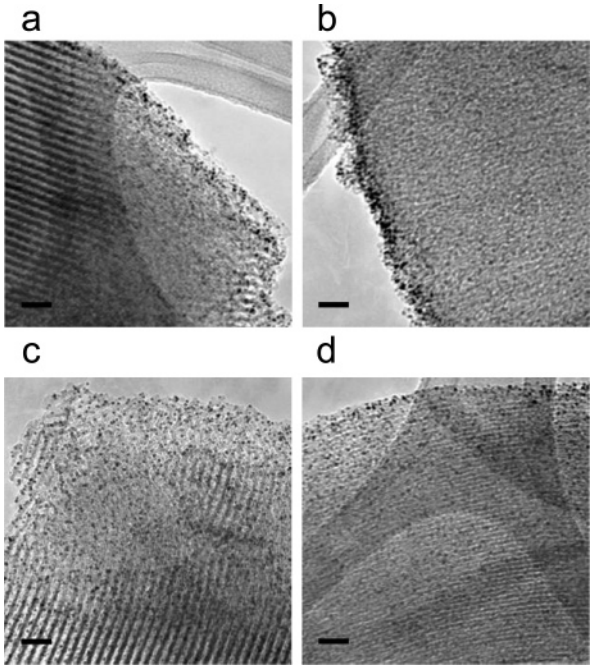

Figure 9. TEM images of Pt/SBA-15 sonicated for various times at room temperature in water/ethanol (1:1) mixture: (a) for 3 min,. (b) for 10 min, (c) for 30 min, (d) for 90 min. The scale bars represent 20 nm.

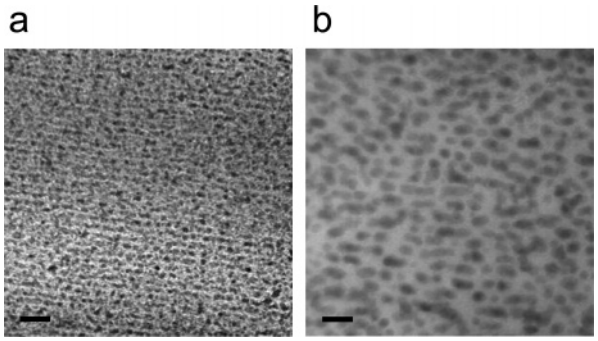

Figure 10. TEM images of 14.4 wt % Pt (2.9 nm)/SBA-15: (a) before H_2 treatment, and (b) after treatment with H_2 flow at 673 K for 75 min. The scale bars represent 20 nm.

confirms that most of the Pt particles in Pt/SBA-15 are located inside the mesopores. It appears that the Pt particles in 0.95% Pt (2.9 nm)/SBA-15 are primarily located inside the channels, although the possibility of Pt particles located on the external surface cannot be ruled out.

3.2.3 Particle Size Determination by Chemisorption Measurement. Particle size determinations by TEM and XRD are in excellent agreement. While these techniques are bulk measures of particle size, we have measured the particle size of the supported Pt crystallites using selective chemisorption measurements. Boudart[17] has suggested that the most pertinent normalization of catalytic activity to a turnover frequency basis should be done with chemisorption measurements rather than electron microscopy or XRD.

The dispersion or ratio of surface atoms to the total number of atoms was determined for all ~1% Pt/SBA-15 catalysts. A summary of the chemisorption data for all catalysts is compiled in Table 1. Monolayer values were obtained by extrapolating isotherms to zero pressure. Dispersions for all catalysts were determined using four separate methods: H_2 chemisorption, CO chemisorption, O_2 chemisorption, and H_2–O_2 titration ($Pt_s-O + {}^3/_2H_2 \rightarrow Pt_s-H + H_2O$).[18] The well accepted 1:1 surface hydrogen metal atom stoichiometry was used to count the number of surface atoms by H_2.[19] The reported dispersion based on H_2 chemisorption and H_2-O_2 titration for the Pt/SBA-15 series was based on the total, rather the irreversible (strong) uptakes. Boudart[20] has suggested that the total rather than the irreversible uptake is a better measurement of Pt surface area when Pt is not highly dispersed. For CO chemisorption, the surface reaction was assumed to occur with a 1:1 stoichiometry. Carbon monoxide adsorbs predominantly in the linear form on Pt at ambient temperatures and high pressures of CO.[21] Oxygen was assumed to adsorb dissociatively at room temperature.

Fractional dispersions for the Pt/SBA-15 series range from 0.13 to 0.31 based on total H_2-O_2 titration uptakes for supported as-synthesized Pt particles ranging from 1.7 to 7.1 nm. The four separate measurements are in good agreement when compared for the same sample. A 3.2% Pt/SiO_2 catalyst prepared by ion exchange (Pt/SiO_2-IE)[22] used as a standard had an irreversible measured uptake corresponding to a dispersion greater than unity. Spenadel and Boudart[23] have suggested it is unlikely that Pt is truly atomically dispersed because it would be difficult to account for the rapid uptake of one hydrogen atom per platinum atom. The lack of any Pt reflections in the X-ray diffraction pattern confirms that the Pt particles are very small (<2.5 nm). A value of unity for metallic dispersion was used for the 3.2% Pt/SiO_2-IE in calculations of turnover frequency for ethane or methane formation in ethylene hydrogenation and ethane hydrogenolysis, respectively.

The Pt particle size based on chemisorption was calculated according to the equation d (nm) = 1.13/D, where D is the metallic dispersion. The above equation assumes spherical particles and a Pt atom density of 1.25×10^{19} atoms m^{-2}.[24] From Table 1, it can be seen that the Pt particle size calculated from chemisorption trends with the TEM particle size of the free-standing particles. XRD measurements on the supported Pt/SBA-15 particles indicated that the Pt particles were not agglomerated by sonication or the pretreatment procedure; however, as shown in Table 1, there is a significant difference in the measured particle size between the two techniques (chemisorption and XRD). While the two techniques measure average particle size, their averages (surface versus volume) are different, but often good agreement between the two is found when the Pt particle size is in the range in which the line-broadening technique is applicable.[23] Two possible explanations exist to explain this large discrepancy in particle size. Synthesis of the Pt nanoparticles requires the use of a template polymer that prevents particles from agglomerating while in solution. Consequently, this polymer (PVP in our synthesis) bonds very strongly to the Pt surface and is difficult to remove after the particles have been dispersed within the SBA-15 matrix. A polymer removal method based on thermal calcination that leads to no particle agglomeration has been developed. Although the calcination procedure has been optimized, a possible explanation for the discrepancy between chemisorption and XRD particle size is a reduced exposed surface area due to the existence of remaining polymer on the Pt surface. XRD would be insensitive to this circumstance, while chemisorption would directly probe this loss of surface area. Spectroscopic data (both infrared and Raman) show no absorption bands attributable to PVP, although it cannot be ruled out that the Pt surface is covered with carbon. There is no apparent advantage of using calcination times longer than 12 h (7.1 nm as an exception).

An important consequence to note about comparison of the free-standing TEM particle and that determined by selective

TABLE 1. Probe Gas Uptake and Average Particle Size for the Pt/SBA-15 Catalysts

		probe gas uptakes[c] (μmol g^{-1})						particle size, d (nm)		
			CO			H_2-O_2	dispersion, D,	chemisorption[d]		
catalyst[a]	TEM particle size[b]	H_2 total	total	irrev	O_2 irrev	total	H_2-$O_{2,\ total}$	H_2	H_2-O_2	XRD[e]
Pt powder		12.3	7.1	6.9	4.0	17.2	0.0022	235	505	> 100
3.2% Pt/SiO_2−IE		133.1	166.7	152.2	24.2	262.0	1[f]	<1	<1	
0.73% Pt/SBA-15	1.7	7.4	13.3	12.2	4.3	17.4	0.311	2.9	3.6	
0.90% Pt/SBA-15	2.6	3.9	9.4	9.4	3.2	22.2	0.321	6.6	3.5	2.5
0.95% Pt/SBA-15	2.9	6.8	7.8	7.8	2.6	18.1	0.248	4.1	4.6	3.0
0.46% Pt/SBA-15	3.6	3.7	5.0	3.9	1.6	12.9	0.364	3.5	3.1	3.8
1.0% Pt/SBA-15	3.6	4.0	9.6	9.3	2.6	15.6	0.203	7.1	5.6	3.8
1.01% Pt/SBA-15	7.1	2.1	5.0	4.6	2.2	10.1	0.131	8.7	8.7	7.8

[a] Elemental analyses determined by ICP-MS. [b] Number-average particle size. Determined by counting a minimum of 200 free-standing particles. [c] Conducted at 295 K. [d] Determined by 1.13/(Pt_s/Pt_T). [e] Based on the Scherrer equation after subtracting SBA-15 baseline. [f] Dispersion, $D = 1$ if $Pt_s/Pt_T > 1$.

TABLE 2. Reaction Rate and Kinetic Data for Ethylene Hydrogenation on Pt/SBA-15 Catalysts

					reaction orders	
catalyst[a]	TEM particle size[b] (nm)	activity[c] (μmol g^{-1} s^{-1})	TOF[c,d] (s^{-1})	E_a[e] (kcal mol^{-1})	C_2H_4[f]	H_2[g]
3.2% Pt/SiO_2−IE	-	123.34[h]	0.752[h]	7.1	−0.2	0.86
0.73% Pt/SBA-15	1.7	8.3	0.710	6.9	0.1	0.75
0.90% Pt/SBA-15	2.6	9.8	0.659	7.4	0.08	0.72
0.95% Pt/SBA-15	2.9	8.5	0.703	7.9	0.05	0.77
0.46% Pt/SBA-15	3.6	5.9	0.683	7.6	0.08	0.7
1.0% Pt/SBA-15	3.6	6.7	0.644	6.9	0.11	0.69

[a] Elemental analyses determined by ICP-MS. [b] Number-average particle size. Determined by counting a minimum of 200 free-standing particles. [c] Reaction conditions were 10 Torr C_2H_4, 100 Torr H_2, and 298 K. [d] Surface Pt (Pt_s) determined from total H_2-O_2 titration. [e] Reaction conditions were 10 Torr C_2H_4, 100 Torr H_2, and 273−313 K. [f] Reaction conditions were 6−40 Torr C_2H_4, 150 Torr H_2, and 298 K. [g] Reaction conditions were 10 Torr C_2H_4, 100−500 Torr H_2, and 298 K. [h] Rate extrapolated from 227 K assuming $E_a = 7$ kcal mol^{-1} and temperature-independent reaction orders.

chemisorption is that some portion of the supported Pt nanoparticle is involved in bonding with the silica surface and will be unable to chemisorb gas. With the construction of the appropriate geometrical picture of the metal−support interface, the difference in particle size between XRD and chemisorption measurements could potentially be used to calculate the interfacial area between the Pt nanoparticle and mesoporous SBA-15 silica.

3.3 Ethylene Hydrogenation on Pt/SBA-15 Catalysts. *3.3.1 Comparison of Activity and Kinetic Parameters with Other Model Systems.* Ethylene hydrogenation was chosen as a test reaction to compare the activity of Pt/SBA-15 materials with kinetic measurements made on supported Pt catalysts prepared by standard preparation techniques (i.e., incipient wetness, ion-exchange) and other model systems such as single crystals and nanoparticle arrays. Table 2 is a compilation of the turnover rates (at standard conditions) measured on a number of catalysts used in this study including a Pt powder (Alfa Aesar, 99.9%, 1 μm particle size). Turnover frequencies at standard conditions (10 Torr C_2H_4, 100 Torr H_2, 298 K) for the Pt/SBA-15 catalysts are ~0.7 s^{-1}. Pristine SBA-15 and the quartz diluent had no activity for ethylene hydrogenation over the entire temperature range of this study (273−313 K). The apparent activation energy for this reaction is low (~6−7 kcal mol^{-1}). Turnover frequencies for all catalysts with particle sizes ranging from 1.7 to 7.1 nm were the same, confirming the well-known structure insensitivity of this reaction. Table 3 is a compilation of turnover frequencies for ethylene hydrogenation over selected classical high-surface-area supported catalysts and model systems. A complete compilation of ethylene hydrogenation kinetics on metallic catalysts can be found elsewhere.[25] Both the Pt(111) single crystal and Pt nanoparticle arrays are more active than the Pt/SBA-15 catalysts by an order of magnitude. Rates measured on our monodispersed nanocatalysts (Pt/SBA-15 series) are in very good agreement with measurements on classical high-surface-area supported catalysts.

TABLE 3. Compilation of Turnover Frequencies for Ethylene Hydrogenation on Model Catalysts and Selected Classical High-Surface-Area Supported Catalysts

catalyst	turnover frequency[a,b] (s^{-1})	E_a (kcal mol^{-1})	reference
Pt/SBA-15	~0.7	~7	this work
Pt(111)	9.3	10.8	25
Pt nanoparticle array	14.3	10.2	26
0.04% Pt/SiO_2	4.4	8.6	27
Pt wire	2.7	8.6	27
Pt wire	3.5	10.0	28
0.05% Pt/SiO_2	0.0037	16.0	29
0.05% Pt/SiO_2	0.0029	17.0	30
2.45% Pt/SiO_2	9.3	10.5	31
Pt film (evaporated)	50.5	10.7	32
0.05% Pt/SiO_2	1.3	9.1	33
0.5% Pt/SiO_2	17.5	8.9	33
9.2% Pt/Al_2O_3	53.4	10.0	34

[a] Rates corrected to 10 Torr C_2H_4, 100 Torr H_2, and 298 K. [b] Corrected assuming zero order and first order dependence for ethylene and H_2, respectively.

The Madon−Boudart (MB) test[13] was used to verify the absence of heat and mass transfer effects during the room-temperature hydrogenation of ethylene in a differential PFR. The MB test requires measurement of the reaction rate (on per gram basis) for catalysts with varying surface concentrations of metal but with similar dispersion. A log−log plot of rate versus surface concentration should yield a straight line with a slope equal to one, if heat and mass transfer effects are absent. For an exothermic reaction, the test should be repeated at a second temperature. In accordance with the criteria of the MB test, the rate was measured using catalysts with different metal loading but similar dispersion (determined by H_2-O_2 titration)

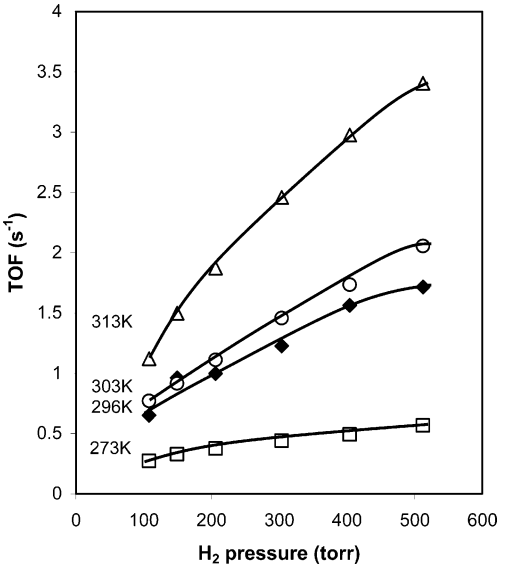

Figure 11. Temperature dependence (273−313 K) of H_2 partial pressure for ethylene hydrogenation on a 1.0% Pt (3.6 nm)/SBA-15. Reaction conditions were 10 Torr C_2H_4, and 100−500 Torr H_2. Lines are drawn in for clarity.

at two different temperatures. The slope of the line (not shown) at both temperatures is ∼1 verifying that the measured rate is independent of the influence of transport effects.

Table 3 also contains a compilation of apparent activation energies for a number of model systems and some selected examples of classically prepared (i.e., incipient wetness, ion exchange) heterogeneous catalysts. It is well-known that ethylene hydrogenation occurs at room temperature and below, which suggests that the true activation energy for the reaction is quite low. For all catalysts used in this study, the apparent activation energy was ca. 7 kcal mol^{-1}, which is slightly lower than previously reported values on low loaded Pt/SiO_2 catalysts (9 kcal mol^{-1}),[26] electron beam lithography Pt nanoparticle arrays (10.2 kcal mol^{-1}),[27] and a Pt(111) single crystal (10.8 kcal mol^{-1}).[28] Reaction orders in hydrogen are ∼0.6 at 298 K. These are higher than the H_2 order (0.5) predicted based on the Horiuti−Polanyi mechanism,[29] which assumes gas-phase hydrogen and surface H atoms are in equilibrium. The apparent H_2 reaction order is temperature-dependent, as shown in Figure 11. As the temperature increases from 273 to 313 K, the reaction order in hydrogen increases from 0.45 to 0.7. Reaction orders in hydrogen on the same series of Pt/SBA-15 catalysts at 195 K are ∼0.4. In a study of ethylene hydrogenation on Pt/SiO_2 catalysts, Cortright and co-workers[30] have shown that the hydrogen order increased from 0.48 to 1.10 as the temperature was increased from 223 to 336 K, at 25 Torr C_2H_4 and hydrogen pressures ranging from 50 to 650 Torr. At low temperatures and high ethylene pressures, the observed reaction-order dependency for both ethylene and hydrogen can be explained by a Horiuti−Polanyi mechanism in which hydrogen is adsorbed noncompetitively on a surface essentially covered with adsorbed hydrocarbon species.

The olefin generally has an inhibiting effect on the overall reaction rate in olefin hydrogenation reactions.[31] The olefin displaces hydrogen from the metal surface, negatively impacting the measured reaction rate as the olefin pressure is increased. At lower ethylene pressures and higher temperatures, more adsorption sites are available for hydrogen and a maximum in ethylene hydrogenation activity is seen on Pt catalysts. The apparent reaction order in ethylene is temperature-dependent (not shown). At room temperature, the dependence on ethylene is zero order or slightly positive, while at higher temperatures, the reaction order approaches −0.3. As the temperature is increased and total surface coverage decreases, the ethylene order becomes more negative, suggesting that the adsorption between ethylene and hydrogen becomes competitive. Cortright and co-workers[30] have measured a similar trend with temperature, and have separately assembled a microkinetic model.[32] Assuming a mechanism in which H_2 could adsorb dissociatively on a surface site in direct competition with ethylene or on a noncompetitive adsorption site, the microkinetic model is able to predict the experimentally observed reaction orders over a 100 K range.[32] El-Sayed and co-workers have shown that the reaction order in propylene during propylene hydrogenation is ∼0.1 at 313 K.[33] In fact, a reaction order of ∼0.2 for ethylene on the Pt/SBA-15 catalysts at 195 K has been measured. At these low temperatures, on the Pt/SBA-15 catalysts, it appears that ethylene is in direct competition with hydrogen for adsorption sites and ethylene hydrogenation is not occurring over the hydrocarbon-covered fraction of the surface.

Horiuti and Polanyi[29] proposed a reaction mechanism that involved the sequential hydrogenation of a surface olefin species, which involved the formation of a surface half-hydrogenated species (i.e., ethyl in the case of ethylene hydrogenation). Zaera and Somorjai demonstrated that the hydrogenation of ethylene on Pt(111) occurs on a hydrocarbon-covered surface.[28] Ethylidyne (≡C−CH_3) was identified as a spectator species that turns over orders of magnitude slower than the presumed reaction intermediate, π-bonded ethylene.[34] Somorjai and co-workers suggest that the ethylidyne layer covers the surface upon which ethylene adsorbs and H_2 is adsorbed dissociatively on the Pt surface.[35] Electron energy loss spectroscopy studies of ethylene hydrogenation on Pt(111) at 298 K demonstrated that the Pt(111) surface is covered with ethylidyne and ethyl radicals.[36] The ethyl radicals were easily hydrogenated, which suggests they are a reaction intermediate to ethane formation. Dumesic and co-workers have shown that the formation of ethylidyne is not necessary for the hydrogenation of ethylene on supported Pt particles.[37] Beebe and Yates[38] have shown that under hydrogen-rich conditions, surface ethylidyne is not necessary for ethane formation over supported Pd catalysts. It appears that there is still much debate over the mechanism of ethylene hydrogenation, but it is clear that the mechanism changes with temperature and partial pressure of both ethylene and hydrogen, and our nanocatalysts display behavior similar to that of classical catalyst systems when ethylene and hydrogen pressures are varied.

3.4 Ethane Hydrogenolysis. The hydrogenolysis of ethane is one of the most fundamental reactions studied in heterogeneous catalysis. The importance of studying such a reaction is noted by considering that two of the most important processes in heterogeneous catalysis are occurring in one reaction: C−H and C−C bond activation. The high temperatures required for ethane hydrogenolysis signifies the strength of the C−C bond because it is well-known that H/D exchange on ethane occurs at temperatures significantly lower than those required for measurable hydrogenolysis activity.[39] Anderson and Kemball[40] have shown that H/D exchange on Pt films occurs at ∼430 K with an apparent activation energy of 22 kcal mol^{-1}. Zaera and Somorjai have shown that deuterium exchange rates were 3 orders of magnitude higher than the rate of ethane hydrogenolysis on Pt(111) at 550 K.[41]

3.4.1 Comparison of Hydrogenolysis Activity and Kinetic Parameters with Classical Supported Catalyst. The hydrogenolysis of ethane on the Pt/SBA-15 catalysts was studied in a PFR at temperatures of 613−653 K under high hydrogen

TABLE 4. Reaction Rate and Kinetic Data for Ethane Hydrogenolysis on Pt/SBA-15 Catalysts

catalyst[a]	TEM particle size[b] (nm)	activity[c] (μmol g^{-1} s^{-1})	TOF[d] 100 × (s^{-1})	E_a (kcal mol^{-1})	reaction orders C_2H_6[f]	reaction orders H_2[g]
Pt powder		0.508	4.51	54.0	0.90	−2.2
3.2% Pt/SiO2−IE		2.356	1.44	65.3	0.98	−2.6
0.73% Pt/SBA-15	1.7	0.159	1.36	48.9	0.70	−1.87
0.90% Pt/SBA-15	2.6	0.155	1.05	54.6	0.70	−1.84
0.95% Pt/SBA-15	2.9	0.110	0.91	53.9	0.65	−1.92
1.0% Pt/SBA-15	3.6	0.091	0.87	56.7	0.74	−1.91
1.01% Pt/SBA-15	7.1	0.035	0.52	48.9	0.75	−1.92

[a] Elemental analyses determined by ICP-MS. [b] Number-average particle size. Determined by counting a minimum of 200 free-standing particles. [c] Reaction conditions were 20 Torr C_2H_6, 200 Torr H_2, and 643 K. [d] Based on total H_2-O_2 titration. [e] Reaction conditions were 20 Torr C_2H_6, 200 Torr H_2, and 613−653 K. [f] Reaction conditions were 18−55 Torr C_2H_6, 200 Torr H_2, and 643 K. [g] Reaction conditions were 32 Torr C_2H_6, 80−300 Torr H_2, and 643 K.

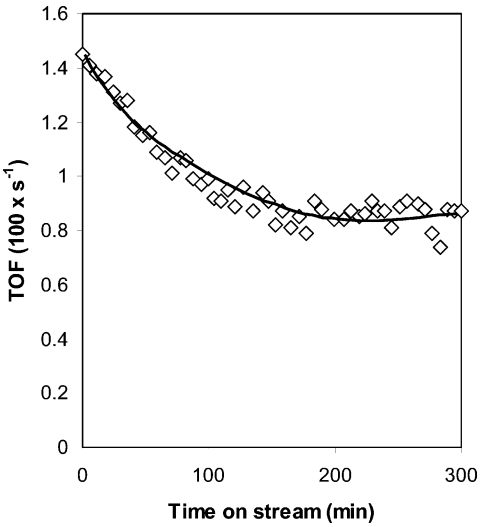

Figure 12. Time on stream behavior of 1% Pt (3.6 nm)/SBA-15 catalyst during ethane hydrogenolysis. Rates corrected to 20 Torr C_2H_6, 200 Torr H_2, and 643 K.

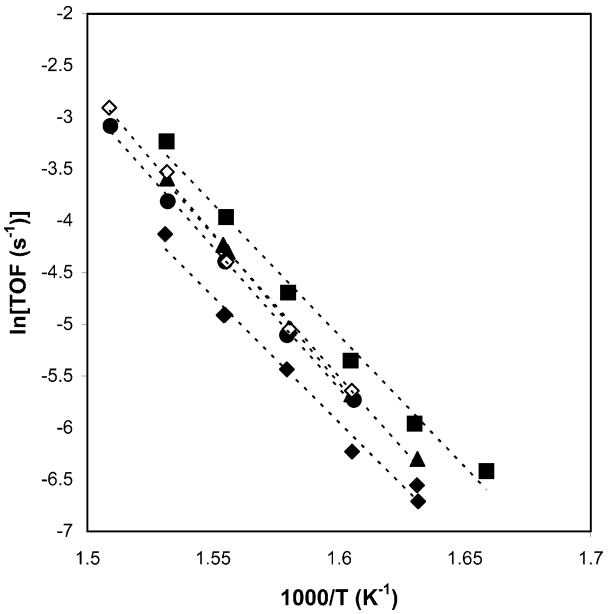

Figure 13. Arrhenius plot for ethane hydrogenolysis. Reaction conditions were 20 Torr C_2H_6, 200 Torr H_2, and 613−653 K: (■) 1.7 nm, (▲) 2.6 nm, (◇) 3.6 nm, (◆) 7.1 nm.

partial pressures. Freshly reduced catalysts generally deactivated over a 1−2 h time period, after which a steady-state rate was achieved and measured rates were stable for the duration of an experiment. The temporal behavior of ethane hydrogenolysis for a 1% Pt (3.6 nm)/SBA-15 catalyst is shown in Figure 12. All rates reported represent measured rates after deactivation had subsided. Table 4 is a compilation of turnover frequencies (at standard conditions) and kinetic parameters for this reaction. Turnover frequencies for ethane hydrogenolysis range from 0.52 to 1.44 × 10^{-2} s^{-1} at 643 K. The turnover frequency for Pt powder was higher by about a factor of 3 for the most active SBA-15 sample, 0.73% Pt (1.7 nm)/SBA-15. The higher turnover frequency may be due to temperature gradients within the catalyst bed. The Pt powder was not diluted and heat transfer effects may influence the rate reported in Table 4. The absence of transport artifacts was confirmed with the MB test for the Pt/SBA-15 catalysts. Cortright and co-workers[42] reported a turnover frequency of 2.4 × 10^{-1} s^{-1} at 643 K for a 2.5% Pt/SiO_2 with a particle size of 1.3 nm, which is an order of magnitude higher than that measured on a Pt/SBA-15 catalyst with comparable Pt particle size. Sinfelt and co-workers[43] measured a turnover frequency of 1 × 10^{-3} s^{-1} on a 10% Pt/SiO_2 catalyst with a particle size of 5 nm. On the Pt/SBA-15 catalysts, the rate is sensitive to the Pt particle size with smaller particles displaying higher activity. It appears from comparison with reported turnover frequencies on high-surface-area supported catalysts that rates differ with particle size. A discussion about the apparent structure sensitivity[44] of ethane hydrogenolysis will be presented later.

The apparent activation energy over the temperature range studied (613−653 K) and a C_2H_6:H_2 ratio of ∼5 varied from 48 to 65 kcal mol^{-1} with average activation energy of ca. 53 kcal mol^{-1} for the Pt/SBA-15 samples (Figure 13). Sinfelt and co-workers measured an apparent activation of 54 kcal mol^{-1} on a 0.6% and 10% Pt/SiO_2 catalyst at similar temperatures and partial pressures of ethane and hydrogen.[43,45] Apparent activation energies for ethane hydrogenolysis have been shown to change due to catalyst supports,[43,46] bimetallic composition,[47,48] and metal surface.[43] The change in activation energy with metal surface is attributed to a change in the rate-determining step[49] and has been correlated with the % *d* character of the metal.[50] The amount of hydrogen has been shown to have a significant influence on the measured apparent activation energy, with the activation energy decreasing as the ratio of C_2H_6:H_2 becomes greater than unity. Gudov et al.[51] determined an apparent activation energy of 47 kcal mol^{-1} when H_2 was present in a 10-fold excess, and 23 kcal mol^{-1} when ethane was in 3-fold excess.

Reaction orders for ethane and hydrogen are ∼0.7 and −1.9, respectively, on the Pt/SBA-15 catalysts at 643 K (see Table 4). The strong negative hydrogen dependence suggests an intense competitive adsorption between hydrogen and ethane on the catalyst surface. Cortright and co-workers have shown that the H_2 order becomes less negative as the temperature is increased (−1.6 at 673 K versus −2.2 at 573 K) or the H_2 partial

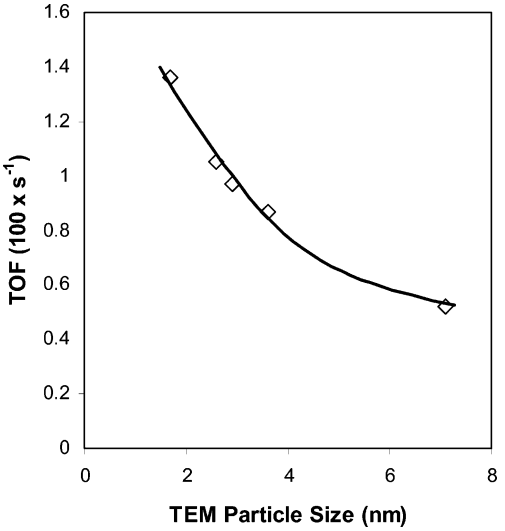

Figure 14. Structure sensitivity of ethane hydrogenolysis on ~1% Pt(*X*)/SBA-15 with Pt particle sizes ranging from $X = 1.7$ to 7.1 nm. Rates corrected to 20 Torr C_2H_6, 200 Torr H_2, and 643 K.

pressure is decreased. A noticeable difference between the Pt/SBA-15 catalysts and both standard samples (Pt powder and Pt/SiO_2−IE) is the degree of hydrogen dependence on the overall rate. The hydrogen reaction order for the two standard catalysts are ≥ -2.2, while the H_2 order for the SBA-15 catalysts is ~ -1.9. One possible explanation for the lower negative dependence on hydrogen is consistent with a previously proposed mechanism in which ethane is adsorbed on chemisorbed hydrogen.[52−54] The apparent reaction order in ethane is consistent with previous experimental observations[55] that for measured reaction orders less negative in H_2, the reaction order in ethane decreases to below one. The ethane reaction order was temperature-dependent, decreasing from 1 to 0 as the temperature was increased from 573 to 673 K at a H_2 partial pressure of 100 Torr, but remained unity when the hydrogen pressure was 350 Torr.[42] Gudkov et al.[51] have shown that the measured reaction order in hydrocarbon and hydrogen can be either positive or negative depending on the conditions, and Cimino et al.[56] have shown that the identity of the metal can influence whether the hydrogen reaction order is positive or negative. Observed partial pressure dependencies are consistent with previously reported values and suggest a mechanism where ethane adsorbs associatively to chemisorbed hydrogen.

3.4.2 Structure Sensitivity of Ethane Hydrogenolysis on Pt. Turnover frequencies for ethane hydrogenolysis varied by a factor of 3 over 1.7−7.1-nm particles with smaller particles having higher activity for the Pt/SBA-15 catalysts (Figure 14). A limited number of studies of ethane hydrogenolysis have been conducted on Pt catalysts. Guczi and Gudkov[57] reported a monotonic decrease in ethane hydrogenolysis on supported Pt particles in the size range of 3−20 nm. Turnover frequency varied from 0.13 to 3×10^{-3} s^{-1} at 523 K with smaller particles demonstrating higher activity. The authors suggest that the increase in rate with smaller particles is related to an increase in the number of corner and edge atoms. Sinfelt and co-workers have measured turnover rates on atomically dispersed Pt particles supported on both Al_2O_3 and SiO_2. Measured turnover frequencies are approximately an order of magnitude lower than those measured in this work.[45] Maximum rates as a function of particle size have also been observed on supported Pt catalysts. In a range of Pt particles of 1.7−5 nm, the specific activity had a clear maximum at 2.5 nm.[58] In fact, similar behavior was observed for propane hydrogenolysis on the same series of catalysts. Ethane hydrogenolysis over Pt/γ-Al_2O_3 catalysts prepared by impregnation methods demonstrated a maximum in rate with particle size although a limited number of samples were studied.[59] Catalysts with atomically dispersed Pt ($d_{Pt} < 1$ nm by H_2 chemisorption) had a turnover frequency of 0.02 s^{-1} at 666 K in excess hydrogen, while the turnover frequency for a catalyst with 1.4-nm particles increased by a factor of 2.5 (0.05 s^{-1}), but decreased to 0.01 s^{-1} after the catalyst was intentionally sintered by thermal treatment.

3.4.3 Ethane Hydrogenolysis Reaction Mechanism and Its Relationship to Structure Sensitivity. A feature common to all proposed mechanisms for ethane hydrogenolysis is that the dehydrogenated C_2H_x species is bonded to more than one metal surface atom, which is dependent upon the degree of ethane dehydrogenation. Dumesic and co-workers have conducted a number of theoretical studies of ethane adsorption on Pt clusters[60,61] and slabs[61] to investigate the interaction of possible C_2H_x intermediates with a Pt surface. Calculations of C_2H_x species adsorbed on a Pt surface suggest that primary pathways for C−C bond cleavage may take place through highly hydrogenated activated complexes, which is contrary to the mechanisms interpreted solely from kinetic measurements.[62,63] For example, the barriers to C−C bond cleavage of the activated complexes of ethyl (C_2H_5) and ethylidene ($CHCH_3$) are 44 and 39 kcal mol^{-1}, respectively, compared with 61 and 79 kcal mol^{-1} for vinyl ($CHCH_2$) and vinylidene (CCH_2) species. Microkinetic analysis[64] has also suggested that C−C bond cleavage takes place through an ethyl (C_2H_5) species, while a $CHCH_3$ species also contributes to C−C bond cleavage. The ethyl radical is the most reactive intermediate, but not the most abundant surface intermediate (*masi*). The highly dehydrogenated species, ethylidyne ($C-CH_3$), is stable on the surface and believed to be the *masi* after adsorbed H ($\theta_H = 0.55$ at 623 K). Examining the hydrogenolysis of ethane over a wide range of experimental conditions, Gudkov suggested that the rate-determining step changes with reaction conditions. At high ratios of hydrogen to ethane, the cleavage of the C−C bond occurs through the ethyl radical, while at low hydrogen-to-ethane ratios, C−C bond breakage occurs in a highly dehydrogenated species.[51] The hydrogenolysis of ethane on Pt single crystals is currently under investigation in our laboratories using sum frequency generation to identify reaction intermediates under relevant turnover conditions.[65]

Boudart has suggested that structure sensitivity/insensitivity may be related to the number of surface atoms to which the critical reactive intermediate is bound.[66] With this definition, a structure-insensitive reaction may be one where the critical intermediate binds through one or two surface atoms. Conversely, a reaction may be classified as structure-sensitive if the critical reactive intermediate is bound to multiple atoms. Single crystals are useful for studying the effect of surface structure on catalytic activity, and are useful analogues for comparison with metal particles in the range of 1−5 nm. A particle size change from 1 to 5 nm is similar to looking at different crystallographic planes on a macroscopic single crystal.[66] Surprisingly, outside of one study,[41] no other kinetic data could be found for the hydrogenolysis of ethane on Pt single crystals.

To understand the role of surface structure on ethane hydrogenolysis, Dumesic and co-workers have studied the reactivity of various C_2H_x species on Pt(111) and Pt(211) slabs using density functional theory methods.[61] The (211) facet is composed of single atom steps of (001) orientation separated by two atom wide terraces of (111) orientation. The calculations

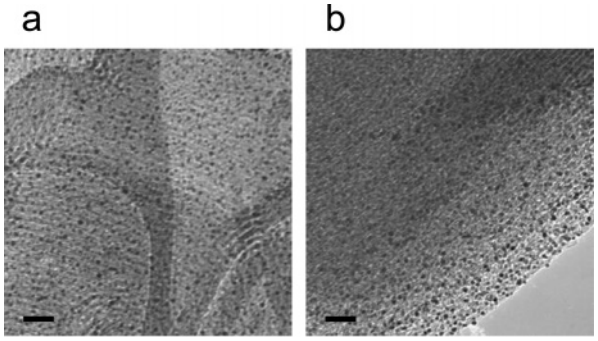

Figure 15. TEM images of 0.95 wt % Pt (2.9 nm)/SBA-15 after reaction: (a) ethylene hydrogenation at 195 K, and (b) ethane hydrogenolysis at 643 K. The scale bars represent 20 nm.

show that the barrier from the stable C_2H_5 adsorbed species to the corresponding activated complex is 17 kcal mol^{-1} lower on Pt(211) than Pt(111), while the Pt(211) is more efficient at stabilizing the C_2H_5 adsorbed species by ~11 kcal mol^{-1}.[60,61] The stable adsorption of C_2H_5 to Pt(221) and Pt(111) occurs through a carbon atop a Pt atom, while the activated C_2H_5 complex is bonded to two Pt atoms on Pt(111). In the case of Pt(211), the activated C_2H_5 complex is bonded through two atoms on the (111) terrace adjacent to the step edge. The binding energy in a 2-fold adsorption site is 28 kcal mol^{-1} stronger for Pt(211) than Pt(111). Small metal crystallites have a higher proportion of coordinatively unsaturated surface atoms, analogous to a stepped single crystal, while the surfaces of large particles primarily expose low index planes (i.e., Pt(111)). It appears that reactions involving these C_2H_x and their activated complexes will occur on these defect sites because they provide more stable bonding. The theoretical calculation supports the observed structure sensitivity of ethane hydrogenolysis on smaller Pt crystallites.

The presence of an adsorbed alkyl layer on the metal surface has been used to explain the structure insensitivity of olefin hydrogenation reactions.[44,66] The presence of this organic layer on the metal surface effectively washes out the original metal surface. In the case, of ethylene hydrogenation, Somorjai and co-workers[34] have shown that under reaction conditions, the surface is covered with ethylidyne, a spectator in the reaction because it turns over orders by magnitude slower than π-bonded ethylene. Theoretical calculations and microkinetic analyses of Dumesic and co-workers have shown that ethylidyne, vinylidene, and hydrogen are the most abundant intermediates on the surface during ethane hydrogenolysis. While ethylidyne and vinylidene are not involved in the primary reaction pathways, they affect the observed kinetic rates through site blocking. The presence of this metal-alkyl may be an additional factor contributing to the weak structure sensitivity for ethane hydrogenolysis on supported Pt nanoparticles.

3.5 Stability of the Pt/SBA-15 Catalysts After Reaction. Pt particles on the Pt/SBA-15 catalysts exhibited excellent thermal stability. There was no detectable agglomeration after ethylene hydrogenation at low temperature (195 K) and ethane hydrogenolysis at high temperature (643 K) (Figure 15). Those observations indicate that this catalyst is a very good model for studying catalytic reactions at relevant turnover conditions.

3.6 Future Prospects for a High-Surface-Area Model Catalyst. Our understanding of heterogeneous catalysis has increased enormously due to studies using model systems. The development of theoretical tools has enabled us to understand experimental results and calculate heterogeneous catalysis phenomena from first principles. In most circumstances, the tools are complimentary and more is learned together rather than individually. The development of a high-surface-area monodispersed metal nanocatalyst is a major development in heterogeneous catalysis research. These materials are model systems of the industrially used materials with the major advantage that they have several properties (i.e., metal particle size and surface structure, particle location within support) that can be rationally tuned. This permits promising experimental studies of structure−activity and more importantly structure−selectivity relationships using multi-path catalyzed reactions such as alkane (*n*-hexane, *n*-heptane) reforming.

4 Summary

Pt nanoparticles with narrow size distributions (i.e., monodispersed) were produced by various solution-based reduction methods and mesoporous SBA-15 silica was produced by well-established hydrothermal reactions. Pt nanoparticles were embedded into the mesoporous silica using low power sonication. The as-synthesized Pt/SBA-15 was calcined under specific conditions to remove the template polymer from the nanoparticle surface and subsequently reduced to remove oxygen from the Pt surface. The reduced Pt/SBA-15 catalysts were characterized by TEM, XRD, and selective chemisorption measurements. TEM and XRD measurements confirm that the as-synthesized Pt particle size is unaffected by sonication, calcination, or reduction, but particle sizes measured by selective chemisorption are larger on average. Ethylene hydrogenation and ethane hydrogenolysis were used as test reactions to compare the activity of our high-surface-area monodispersed metal nanocatalysts with classical high-surface-area catalysts. Turnover rates for room-temperature hydrogenation of ethylene were identical to a Pt/SiO_2 catalyst made by ion exchange and in good agreement with single-crystal measurements, confirming the structure insensitivity of this reaction. Ethane hydrogenolysis rates were comparable to rates on Pt powder and an ion-exchanged Pt/SiO_2 catalyst. The Pt/SBA-15 catalysts demonstrated weak structure sensitivity, with smaller particles demonstrating higher activity. These catalysts exhibited excellent thermal stability under relevant turnover conditions. The synthesis of these catalysts is a general procedure which enables numerous metal/support systems to be constructed for the study of structure−selectivity correlations in heterogeneous catalysis.

Acknowledgment. This work is supported by the Director, Office of Energy Research, Office of Basic Energy Sciences, Materials and Chemical Sciences Divisions of the U. S. Department of Energy under Contract DE-AC03-76SF00098. We thank Professor M. A. Vannice of the Pennsylvania State University for the 3.2% Pt/SiO_2-IE material and Samrat Mukherjee for preparation of the material. R.M.R. acknowledges the Ford Motor Company and the Berkeley Catalysis Center for financial support. H.S. thanks the Korea Science and Engineering Foundation (KOSEF) for support under the Post-doctoral Fellowship Program.

References and Notes

(1) Strongin, D. R.; Carrazza, J.; Bare, S. R.; Somorjai, G. A. *J. Catal.* **1987**, *103*, 213.
(2) Mohr, C.; Hofmeister, H.; Radnik, J.; Claus, P. *J. Am. Chem. Soc.* **2003**, *125*, 1905.
(3) Farias, M. H.; Gellman, A. J.; Somorjai, G. A.; Chianelli, R. R.; Liang, K. S. *Surf. Sci.* **1984**, *140*, 181.
(4) Sinfelt, J. H.; Hurwitz, H.; Rohrer, J. C. *J. Phys. Chem.* **1960**, *64*, 892.
(5) Hayek, K.; Kramer, R.; Paál, Z. *Appl. Catal. A.* **1997**, *162*, 1.
(6) Weisz, P. B. *Pure. Appl. Chem.* **1980**, *52*, 2091.

(7) Kónya, Z.; Puntes, V. F.; Kiricsi, I.; Zhu, J.; Alivisatos, A. P.; Somorjai, G. A. *Catal. Lett*. **2002**, *81*, 137.
(8) Kónya, Z.; Puntes, V. F.; Kiricsi, I.; Zhu, J.; Alivisatos A. P.; Somorjai, G. A.; *Nano Lett*. **2002**, *2*, 907.
(9) Teranish, T.; Hosoe, M.; Tanaka, T.; Miyake, M. *J. Phys. Chem. B* **1999**, *103*, 3818.
(10) Wang, Y.; Ren, J.; Deng, K.; Gui, L.; Tang, Y. *Chem. Mater*. **2000**, *12*, 1622.
(11) Zhao, D.; Huo, Q.; Feng, J.; Chmelka, B. F.; Stucky, G. D. *J. Am. Chem. Soc.* **1998**, *120*, 6024.
(12) Berger, R. J.; Pérez-Ramíréz, J.; Kapteijn, F.; Moulijn, J. A. *Chem. Eng. Sci*. **2002**, *57*, 4921.
(13) Madon, R. J.; Boudart, M. *Ind. Eng. Chem. Fundam*. **1982**, *21*, 438.
(14) Song, H.; Kim, F.; Connor, S.; Yang, P. **2004**, submitted for publication.
(15) Huang, M. H.; Choudrey, A.; Yang, P. *Chem. Commun.* **2000**, 1063.
(16) Janssen, A. H.; Yang, C.-M.; Wang, Y.; Schüth, F.; Koster, A. J.; de Jong, K. P. *J. Phys. Chem. B* **2003**, *107*, 10552.
(17) Boudart, M.; Djéga-Maraidassou, G. *Kinetics of Heterogeneous Catalytic Reactions*; Princeton University Press: Princeton, NJ, 1984.
(18) Benson, J. E.; Boudart, M. *J. Catal.* **1965**, *4*, 704.
(19) Sinfelt, J. H.; Yates, D. J. C. *J. Catal*. **1968**, *10*, 362.
(20) Vannice, M. A.; Benson, J. E.; Boudart, M. *J. Catal*. **1970**, *16*, 348.
(21) Yates, D. J. C.; Sinfelt, J. H. *J. Catal*. **1967**, *8*, 348.
(22) Singh, U. K.; Vannice, M. A. *J. Catal*. **2000**, *191*, 165.
(23) Spenadel, L.; Boudart, M. *J. Phys. Chem.* **1960**, *64*, 204.
(24) Anderson, J. R.; *Structure of Metallic Catalysts*; Academic Press: New York, 1975.
(25) Horiuti, J.; Miyahara, K. *Hydrogenation of Ethylene on Metallic Catalysts*; NSRDS-NBS 13; National Bureau of Standards; U. S. Government Printing Office: Washington, DC, 1968.
(26) Schlatter, J. C.; Boudart, M. *J. Catal*. **1972**, *24*, 482.
(27) Grunes, J.; Zhu, J.; Anderson, E. A.; Somorjai, G. A. *J. Phys. Chem. B* **2002**, *106*, 11463.
(28) Zaera, F.; Somorjai, G. A. *J. Am. Chem. Soc*. **1984**, *106*, 2288.
(29) Horiuti, I.; Polanyi, M. *Trans. Faraday Soc*. **1934**, *30*, 1164.
(30) Cortright, R. D.; Goddard, S. A.; Rekoske, J. E.; Dumesic, J. A. *J. Catal*. **1991**, *127*, 342.
(31) Bond, G. C. *Heterogeneous Catalysis: Principles and Applications*, 2nd ed.; Oxford Science Publication: New York, 1987.
(32) Rekoske, J. E.; Cortright, R. D.; Goddard, S. A.; Sharma, S. B.; Dumesic, J. A. *J. Phys. Chem.* **1992**, *96*, 1990.
(33) Yoo, J. W.; Hathcock, D. J.; El-Sayed, M. A. *J. Catal*. **2003**, *214*, 1.
(34) Davis, S. M.; Zaera, F.; Gordon, B. E.; Somorjai, G. A. *J. Catal*. **1985**, *92*, 240.
(35) Cremer, P. S.; Su, X. C.; Shen, Y. R.; Somorjai, G. A. *J. Am. Chem. Soc*. **1996**, *118*, 2942.
(36) Backman, A. L.; Masel, R. I. *J. Vac. Sci. Technol. A* **1991**, *9*, 1989.
(37) Goddard, S. A.; Cortright, R. D.; Dumesic, J. A. *J. Catal*. **1992**, *137*, 186.
(38) Beebe, T. P.; Yates, J. T., Jr. *J. Am. Chem. Soc*. **1986**, *108*, 663.
(39) Loazia, A.; Xu, M. D.; Zaera, F. *J. Catal*. **1996**, *159*, 127.
(40) Anderson, J. R.; Baker, B. G. *Proc. R. Soc. (London) A* **1963**, *271*, 402.
(41) Zaera, F.; Somorjai, G. A. *J. Phys. Chem.* **1985**, *89*, 3211.
(42) Cortright, R. D.; Watwe, R. M.; Spiewak, B. E.; Dumesic, J. A. *Catal. Today* **1999**, *53*, 395.
(43) Sinfelt, J. H.; Taylor, W. F.; Yates, D. J. C. *J. Phys. Chem.* **1965**, *69*, 95.
(44) Boudart, M. *Adv. Catal. Relat. Subj*. **1969**, *20*, 152.
(45) Sinfelt, J. H. *J. Phys. Chem*. **1964**, *68*, 344.
(46) Taylor, W. F.; Yates, D. J. C.; Sinfelt, J. H. *J. Phys. Chem*. **1964**, *68*, 2962.
(47) Sinfelt, J. H.; Carter, J. L.; Yates, D. J. C. *J. Catal*. **1972**, *24*, 283.
(48) Sinfelt, J. H. *Acc. Chem. Res.* **1977**, *10*, 15.
(49) Anderson, J. R.; Kemball, C. *Proc. R. Soc. London A* **1954**, *223*, 361.
(50) Sinfelt, J. H.; Yates, D. J. C. *J. Catal*. **1968**, *10*, 362.
(51) Gudkov, B. S.; Guczi, G.; Tétényi, P. *J. Catal*. **1982**, *74*, 207.
(52) Frennet, A. In *Hydrogen Effects in Catalysis*; Paál, Z., Menon, P. G., Eds.; Marcel Dekker: New York, 1988; p 399.
(53) Frennet, A. *Catal. Today* **1992**, *12*, 131.
(54) Frennet, A.; Liénard, G. *J. Chim. Phys. PCB* **1971**, *68*, 1526.
(55) Frennet, A.; Liénard, G.; Crucq, A.; Degols, L. *J. Catal*. **1978**, *53*, 150.
(56) Cimino, A.; Boudart, M.; Taylor, H. *J. Phys. Chem*. **1954**, *58*, 796.
(57) Guczi, L.; Gudkov, B. S. *React. Kinet. Catal. Lett*. **1978**, *9*, 343.
(58) Rhyndin, Y. A.; Kuznetsov, B. N.; Yermakov, Y. I. *React. Kinet. Catal. Lett*. **1977**, *7*, 105.
(59) Cho, I. H.; Park, S. B.; Cho, S. J.; Ryoo, R. *J. Catal*. **1998**, *173*, 295.
(60) Watwe, R. M.; Spiewak, B. E.; Cortright, R. D.; Dumesic, J. A. *J. Catal*. **1998**, *180*, 184.
(61) Watwe, R. M.; Cortright, R. D.; Nørskov, J. K.; Dumesic, J. A. *J. Phys. Chem. B* **2000**, *104*, 2299.
(62) Sinfelt, J. H. *J. Catal*. **1972**, *27*, 468.
(63) Sinfelt, J. H. *Catal. Lett*. **1991**, *9*, 159.
(64) Cortright, R. D.; Watwe, R. M.; Dumesic, J. A. *J. Mol. Catal. A* **2000**, *163*, 91.
(65) Rioux, R. M.; Marsh, A. L.; Somorjai, G. A. Accepted for publication.
(66) Boudart, M. *J. Mol. Catal*. **1985**, *30*, 27.